# Weierstraß-Institut
## für Angewandte Analysis und Stochastik
### Leibniz-Institut im Forschungsverbund Berlin e. V.

Preprint ISSN 2198-5855


# Narrowing of the far field in spatially modulated edge-emitting broad area semiconductor amplifiers


Mindaugas Radziunas[1], Ramon Herrero[2], Muriel Botey[3], Kestutis Staliunas[2,4]



submitted: February 25, 2015



[1] Weierstrass Institute
Mohrenstr. 39
10117 Berlin, Germany
E-Mail: Mindaugas.Radziunas@wias-berlin.de

[2] Departament de Física i Enginyeria Nuclear
Universitat Politècnica de Catalunya
Colom 11
08222 Terrassa, Spain
E-Mail: ramon.herrero@upc.edu

[3] Departament de Física i Enginyeria Nuclear
Universitat Politècnica de Catalunya
Urgell 187
08036 Barcelona, Spain
E-Mail: muriel.botey@upc.edu

[4] Institució Catalana de Recerca
i Estudis Avançats (ICREA)
Pg. Lluís Companys 23
08010 Barcelona, Spain
E-Mail: kestutis.staliunas@icrea.cat



No. 2088
Berlin 2015




2010 *Mathematics Subject Classification.* 35Q60 35B27 78A60 78A45 42B37.

2008 *Physics and Astronomy Classification Scheme.* 42.60.By 42.60.Da 42.60.Fc 42.60.Jf.

*Key words and phrases.* semiconductor amplifier, traveling wave model, coupled mode approach, periodic structure, anisotropy, far field, spatial filtering .

The work of M.R. was supported by EU FP7 ITN PROPHET, Grant No. 264687 and SFB 787 of the DFG.

Edited by
Weierstraß-Institut für Angewandte Analysis und Stochastik (WIAS)
Leibniz-Institut im Forschungsverbund Berlin e. V.
Mohrenstraße 39
10117 Berlin
Germany

Fax: +49 30 20372-303
E-Mail: preprint@wias-berlin.de
World Wide Web: http://www.wias-berlin.de/

**Abstract**

We perform a detailed theoretical analysis of the far field narrowing in broad-area edge-emitting semiconductor amplifiers that are electrically injected through the contacts periodically modulated in both, longitudinal and transverse, directions. The beam propagation properties within the semiconductor amplifier are explored by a (1+2)-dimensional traveling wave model and its coupled mode approximation. Assuming a weak field regime, we analyze the impact of different parameters and modulation geometry on the narrowing of the principal far field component.

# 1 Introduction

High power high brightness edge-emitting semiconductor lasers and amplifiers are compact devices playing a key role in different laser technologies such as free space communications [1], optical frequency conversion [2], three-dimensional printing, marking, materials processing [3], or pumping fiber amplifiers [4]. Edge-emitting broad-area (BA) lasers, which are robust and highly efficient devices for generation of high power beams, however, suffer from a poor spatial beam quality [5]. The stabilization of optical beams in a BA devices can be achieved, for example, by external optical injection [6, 7] or feedback [8, 9]. Most of such suggestions generally relay on an additional optical beams or external cavities rending the device less compact. However, it was recently suggested that introducing an intrinsic 2-dimensional (2D) periodicity on the injected current (as for instance with electrical contacts structured in 2D, on the order of microns) can improve the quality of the beam amplified in the BA device [10, 11].

In this paper we follow this last approach, and theoretically study in detail the far field narrowing mechanism in BA amplifiers of moderate length with a 2D, longitudinal and transverse, modulation of the electrical contacts of the device (see Fig. 1). While for sufficiently long devices the beam profile is solely determined by the most amplified mode, for shorter or moderate lengths a comprehensive analysis of the mode growth show that other modes contribute determining the final beam shape. In this way, a proper choice of the spatial periods can lead to the narrowing of the central far field component while substantially improving the spatial structure of the amplified beam.

Our theoretical study is based on the analysis and simulations of the 1 (time) + 2 (space)-dimensional traveling wave (TW) model which takes into account the spatio-temporal dynamics of slowly varying complex amplitudes of the counter-propagating optical fields, induced polarizations and carrier densities [14, 12, 13]. This modeling approach was already used by us to demonstrate the principle of angular filtering of the moderate-intensity optical beams in BA amplifiers [11].

In order to understand the beam shaping mechanisms in periodically modulated BA amplifiers, we assume that the optical fields remain small and reduce the basic TW model to the linear 2-dimensional Schrödinger equation with 2D-periodic potential. In the next step of simplifications, we reduce this problem to the system of coupled mode (CM) equations, which is a linear system

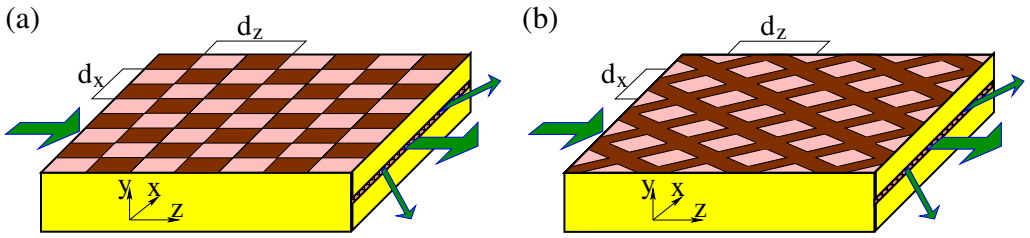


Figure 1: Schematic representation of the simulated BA semiconductor amplifiers with the chessboard-type electrical contact (a) and the fishnet-type contacts (b).

of three ordinary differential equations with the coefficients depending on the radiation angles, modulation periods and amplitude. The CM equations are used to study the dependence of beam angular shaping on different BA device parameters such as device length, linewidth enhancement factor, or amplitude and periods of periodic potential (injected current and periods of modulated contact). The analysis of the CM equations is confirmed by numerical simulations of the BA amplifier using the general TW model.

## 2 Traveling wave model

The TW model describing longitudinal-transverse dynamics of the complex slowly varying amplitudes of the counter-propagating fields $E^{\pm}(z,x,t)$, polarization functions $P^{\pm}(z,x,t)$ and real carrier density function $N(z,x,t)$ in edge-emitting BA lasers and amplifiers is given as follows [12, 13]:

$$\begin{aligned}
&\tfrac{n_g}{c_0}\tfrac{\partial E^{\pm}}{\partial t} \pm \tfrac{\partial E^{\pm}}{\partial z} = \tfrac{-i}{2k_0\overline{n}}\tfrac{\partial^2 E^{\pm}}{\partial x^2} + (\beta - \mathcal{D})\,E^{\pm},\\
&\mathcal{D}E^{\pm} = \tfrac{\overline{g}}{2}(E^{\pm} - P^{\pm}),\ \tfrac{\partial P^{\pm}}{\partial t} = \overline{\gamma}\,(E^{\pm} - P^{\pm}) + i\overline{\omega}P^{\pm},\\
&\tfrac{\partial N}{\partial t} = D_N\tfrac{\partial^2 N}{\partial x^2} + \tfrac{\bar{J}\cdot(1+\zeta(z,x))}{qd} - R(N) - \tfrac{c_0}{n_g}\,\mathrm{Re}\sum_{\nu=\pm}E^{\nu *}\left[\tfrac{g(N)}{1+\varepsilon\|E\|^2} - 2\mathcal{D}\right]E^{\nu}.
\end{aligned} \tag{1}$$

Here $z$, $x$ and $t$ are longitudinal, transverse and time coordinates, $\|E\|^2 = |E^+|^2 + |E^-|^2$ is a local photon density, $c_0$ and $q$ are the speed of light in vacuum and the electron charge, $\lambda_0$ and $k_0 = \frac{2\pi}{\lambda_0}$ are the central wavelength and the corresponding wavenumber in vacuum, the operator $\mathcal{D}$ and parameters $\overline{g}$, $\overline{\gamma}$, $\overline{\omega}$ model the Lorentzian approximation of the material gain dispersion [14], whereas $\beta$, $g$, $\tilde{n}$, and $R$ denote the complex propagation factor, the gain, the index change, and the carrier recombination, respectively:

$$\begin{aligned}
&\beta(N,\|E\|^2) = -\left(\tfrac{\alpha}{2} + i\delta_0\right) + \tfrac{g(N)}{2(1+\varepsilon\|E\|^2)} + i\tilde{n}(N),\\
&g(N) = g' N_{\mathrm{tr}}\ln\left(N/N_{\mathrm{tr}}\right),\ \tilde{n}(N) = k_0\sqrt{\mu N},\ R(N) = AN + BN^2 + CN^3.
\end{aligned} \tag{2}$$

The other parameters used in the formulas above are defined in Table 1.

Whereas the parameter $\bar{J}$ in the carrier rate equation of Eq. (1 denotes the mean injected current density, the function $\zeta(z,x)$ models the spatially periodic electrical contacts of the BA device providing the spatially modulated pump profile. In this paper, the function $\zeta$ is given by

$$\zeta(z,x) = \mathrm{sgn}\Big[\sin(q_z z)\sin(q_x x) + \rho\left(\left|\cos(q_z z)\cos(q_x x)\right| + \cos\left(\tfrac{\pi\sqrt{2}}{2}\right)\right)\Big], \tag{3}$$

where $q_z = 2\pi/d_z$, $q_x = 2\pi/d_x$, and $d_x$ ($d_z$) denotes the transverse (longitudinal) modulation period [11]. The factor $\rho$ determines the considered electrical contact configuration, such that $\rho = 0$ corresponds to the chessboard-type configuration [see Fig. 1(a)] and $\rho = 1$ determines the fishnet case [Fig. 1(b)]. In both cases, $\zeta(z, x)$ has zero mean value (since the area of the contacts equals half the full area of the device), whereas $1$ and $-1$ are the maximal and minimal values of this function.

Table 1: Typical parameter values

| | parameter | value |
|---|---|---|
| $\lambda_0$ | central wavelength | $1$ $\mu$m |
| $n_g$ | group velocity index | $3.6$ |
| $\bar{n}$ | background refractive index | $3.125$ |
| $d$ | depth of the active zone | $15$ nm |
| $w$ | width of the device | $400$ $\mu$m |
| $g'$ | differential gain | $2.5 \cdot 10^{-21}$ m$^2$ |
| $\mu$ | refractive index change factor | $1.0132 \cdot 10^{-31}$ m$^3$ |
| $N_{\mathrm{tr}}$ | transparency carrier density | $1 \cdot 10^{24}$ m$^{-3}$ |
| $\alpha$ | internal absorption | $150$ m$^{-1}$ |
| $\delta$ | static detuning | $0$ m$^{-1}$ |
| $\varepsilon$ | nonlinear gain compression | $5 \cdot 10^{-24}$ m$^3$ |
| $D_N$ | carrier diffusion coefficient | $2.122 \cdot 10^{-3}$ m$^2$/s |
| $A$ | recombination parameter | $0.3 \cdot 10^{9}$ 1/s |
| $B$ | recombination parameter | $2 \cdot 10^{-16}$ m$^3$/s |
| $C$ | recombination parameter | $2.5 \cdot 10^{-42}$ m$^6$/s |
| $\bar{J}$ | mean injection current density | $10$ A/mm$^2$ |
| $d_x$ | transverse period | $8$ $\mu$m |
| $d_z$ | longitudinal period | $400$ $\mu$m |
| $\overline{g}$ | Lorentzian gain amplitude | $10000$ m$^{-1}$ |
| $\overline{\gamma}$ | half width of the Lorentzian | $60$ 1/ps |
| $\overline{\omega}$ | gain peak detuning | $0$ rad/ps |
| $\omega_i$ | frequency of the optical injection | $0$ rad/ps |
| $\sigma_i$ | full width of injected beam power | $20$ $\mu$m |

Along this paper, we consider the unidirectional propagation of optically injected beams in BA amplifiers. Therefore, we neglect field reflections at the semiconductor facets and define the longitudinal boundary conditions for the optical fields, $E^{\pm}$, at the device facets, $z = 0$ and $z = L$, in (1) as

$$E^{+}(0, x, t) = a(x, t), \qquad E^{-}(L, x, t) = 0. \tag{4}$$

This means that the backward propagating field is zero, $E^{-} = 0$. For simplicity, we also assume that the complex amplitude of the optical injection is stationary, while the transverse profile of the injected beam is Gaussian:

$$a(x, t) = a_{st}(x)e^{i\omega_i t} = a_i \exp\left(-x^2 \ln(4)/\sigma_i^2\right) e^{i\omega_i t}. \tag{5}$$

Although the width of the considered device (pumped region), $w$, is finite, the model equations (1) should be considered, in general, in a transverse unbounded domain, since the optical fields (and carrier density function) decay outside the pumped region and vanish for $x \to \pm\infty$. In practice, we consider the model equations in a transversally truncated domain of the width $\geq 1.5\, w$ containing the pumped area, and impose the periodic transverse boundary conditions for $E^{\pm}(z,x,t)$ and $N(z,x,t)$.

Most of the model parameters can be spatially inhomogeneous and discontinuous depending on the device geometry. For instance, $\bar{J}$ is usually non-vanishing within the considered device width, but is set to zero in the rest of the computational domain. More details, meaning and typical values of all parameters are provided in Table 1 and in Refs. [14, 13].

Our major attention is paid to the role of the injection current modulation, determined by the function $\zeta(z,x)$ (3). As it was suggested in Ref. [10], the figure of merit for optical beam quality improvement, during propagation and amplification in 2D-periodically modulated semiconductor BA amplifiers, is given by the following condition:

$$\mathcal{Q} = \frac{2d_x^2\bar{n}}{d_z\lambda_0} = \frac{2k_0\bar{n}q_z}{q_x^2} \approx 1. \tag{6}$$

The values for $\lambda_0$, $\bar{n}$, $d_x$ and $d_z$ in Table 1 exactly fulfill the resonance condition $\mathcal{Q} = 1$. For simplicity, in the following simulations we tune the value of the geometry factor $\mathcal{Q}$ by modifying the background refractive index, $\bar{n}$.

# 3 Reduction of the TW model

In order to analyze the field narrowing in moderate length and moderate power devices we perform a linear approximation of the TW model (1)-(5). We assume a weak injected optical field, $a_{st}(x)$, and determine its propagation and amplification along the BA semiconductor amplifier. We neglect the impact of gain dispersion (omitting polarization functions, $P^{\pm}$, by setting $\overline{g} = 0$) and assume that the propagating field intensity along the amplifier remains small, $\|E\|^2 \ll 1$.

## 3.1 Linear approximation of TW model

As the stimulated recombination term remains negligible, the distribution of the carrier density, $N(z,x,t)$, approaches some spatially modulated stationary state, $N_{st}(z,x)$, determined by the stationary carrier rate equation in (1). A positive real-valued solution of the corresponding spatially-homogeneous equation

$$R(N_0) = \bar{J}/(qd),$$

gives a good approximation for the mean value $N_0$ of $N_{st}(z,x)$. The linearization of the propagation factor $\beta$ around $N_0$, the expansion of the carrier deviation $(N_{st}(z,t) - N_0)$ into the harmonic components with the spatial periods $d_x$ and $d_z$, and a consequent truncation of the higher order harmonics imply the following reasonable approximation for the (stationary) propa-

gation factor $\beta(N_{st},0)$:

$$\begin{aligned}
&\beta(N_{st},0) \approx \beta(N_0,0) + a_m(1+i\alpha_H)V(z,x),\\
&a_m = \frac{-2g'N_{\rm tr}\bar{J}\,\zeta_{1,1}}{qdN_0\left[D_N q_x^2+\frac{\partial R}{\partial N}(N_0)\right]},\quad \alpha_H = \frac{k_0\sqrt{\mu N_0}}{g'N_{\rm tr}},\\
&V(z,x) = \sin(q_z z)\sin(q_x x) + \, b\left[\cos(2q_x x)+b_z\cos(2q_z z)\right],\\
&b = -\frac{\zeta_{0,2}\left[D_N q_x^2+\frac{\partial R}{\partial N}(N_0)\right]}{2\zeta_{1,1}\left[4D_N q_x^2+\frac{\partial R}{\partial N}(N_0)\right]},\; b_z = 1+\frac{4D_N q_x^2}{\frac{\partial R}{\partial N}(N_0)}.
\end{aligned} \tag{7}$$

Here, $\beta(N_0,0)$ , $a_m$, and $\alpha_H$ are the averaged gain/loss and the refractive index change in the amplifier, the modulation amplitude, and the linewidth enhancement factor. $\zeta_{1,1}$ and is the coefficient of the harmonic component $e^{i(q_z z+q_x x)}$ of the function $\zeta(z,x)$. It is, approximately, $-0.405$ and $-0.358$ for the chessboard- and fishnet-type electrical contacts, respectively. Parameter $b$ in the expression of the periodic potential $V$ is proportional to $\zeta_{0,2}$ (the coefficient of the harmonic component $e^{2iq_x x}$ of the function $\zeta(z,x)$), which is strictly positive for the fishnet-type contacts, and vanish in the case of the chessboard contact configuration. More details on the derivation of Eq. (7) can be found in the Appendix.

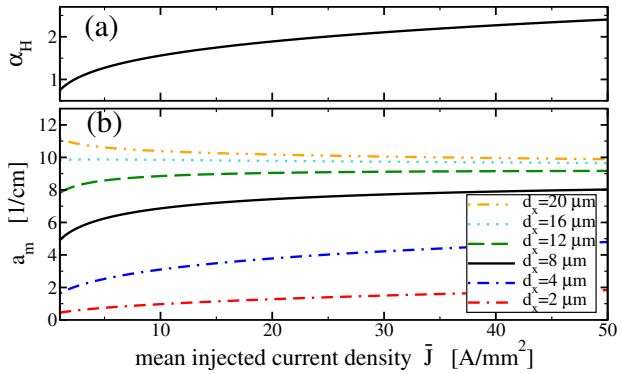


Figure 2: Dependence of the linewidth enhancement factor (a) and modulation amplitude (b) on the mean injected current, $\bar{J}$, according to Eq. (7) for chessboard-type contacts. Parameters as in Table 1.

Panels (a) and (b) of Figure 2 present the estimated dependence of $\alpha_H$ and $a_m$ on $\bar{J}$, respectively. While the linewidth enhancement factor, $\alpha_H$, is uniquely defined by $N_0$, and, therefore, by $\bar{J}$, the modulation amplitude $a_m$ depends also on the transverse modulation period $d_x$. This dependence is due to the carrier diffusion, which efficiently smooths the carrier density distribution in the modulated BA devices with small modulation periods.

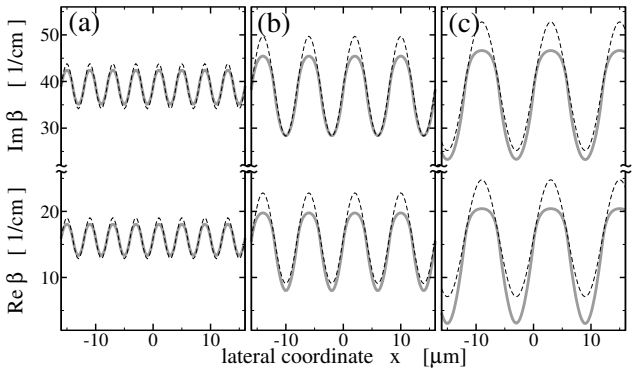


Figure 3: Comparison of the modulated propagation factor in the TW model (1)-(5) [thick gray curves], and its approximation $\beta(N_{st}(d_z/4,x),0)$ from Eq. (7) [black dashed curves] for the chessboard-type modulation. Upper and lower curves represent index and gain variation, respectively. (a) $d_x = 4\,\mu m$. (b) $d_x = 8\,\mu m$. (c) $d_x = 12\,\mu m$. All other parameters as in Table 1.

The consistency of this approximation is proved in Fig. 3, where the thin dashed curves representing the real and the imaginary parts of factor $\beta$ [given by its approximation, Eq. (7)] are compared with the thick gray curves obtained by simulating the TW model (1)-(5). Note that, while in our approximation the gain values, $\mathrm{Re}\,\beta$, are overestimated for large transverse periods, $d_x$, the modulation amplitudes, which are crucial for the beam shaping, are similar to those obtained in the TW model.

In the stationary case, the forward propagating complex optical field evolves according to

$$E^+(z,x,t) = E_0(z,x)e^{i\omega_i t}, \quad \text{i.e.,} \quad \frac{\partial E^+}{\partial t} = i\omega_i E^+.$$

Next, we denote

$$E(z,x) = e^{-\beta(N_0,0)z + i\omega_i(n_g z/c_0 - t)} E^+(z,x,t).$$

The resulting linear problem reads as follows:

$$\frac{\partial E}{\partial z} = \frac{-i}{2k_0\overline{n}}\frac{\partial^2 E}{\partial x^2} + a_m(1+i\alpha_H)V(z,x)E, \qquad E(0,x) = a_{st}(x), \tag{8}$$

where the periodic potential, $V(z,x)$, is defined in Eq. (7).

### 3.2 Coupled mode approximation

Let us express the field function $E(z,x)$ as a superposition of three modal components:

$$E(z,x) = e^{-ik_x x}\langle \vec{a}(z,k_x)\cdot(1, e^{iq_z z - iq_x x}, e^{iq_z z + iq_x x})^T\rangle,$$

where $^T$ stands for transpose, $\vec{a} = (a_0, a_{+1}, a_{-1})^T$, and $\langle\zeta\cdot\xi\rangle$ denotes a standard dot-product of the vectors $\zeta$ and $\xi$. Substituting this ansatz into Eq. (8), taking into account that $q_z = \frac{\mathcal{Q}q_x^2}{2k_0\overline{n}}$, and excluding fast rotating terms, we arrive to the coupled mode (CM) approximation, which consists of the following homogeneous system of CM equations:

$$\begin{gathered}\frac{d\vec{a}}{dz} = \frac{iq_x^2}{2k_0\overline{n}}\begin{pmatrix} s^2 & c & -c \\ c & s^2 - v + 2s & 2cb \\ -c & 2cb & s^2 - v - 2s \end{pmatrix}\vec{a}, \\ s = \frac{k_x}{q_x}, \quad v = \mathcal{Q} - 1, \quad c = \frac{k_0\overline{n}(\alpha_H - i)a_m}{2q_x^2}.\end{gathered} \tag{9}$$

It is noteworthy, that $v$ denotes the deviation from the geometric resonance condition, $\mathcal{Q} = 1$, whereas $s$ is proportional to the field propagation angles inside and outside the semiconductor, $\theta_s \approx \frac{q_x s}{k_0\overline{n}}$ and $\theta_o \approx \frac{q_x s}{k_0} = \frac{k_x}{k_0}$, respectively.

## 4 Analysis of the coupled mode equations

Once the wavevector domain representation $G(k_x)$ of the injected beam $a_{in}(x)$ has vanishing tails for $|k_x| \geq q_x/2$, we can write the solutions of (9) as:

$$\vec{a}(z,k_x) = G(k_x)\sum_{j=1}^{3}\vec{A}^{(j)}e^{-ik_z^{(j)}z}. \tag{10}$$

Here, $-ik_z^{(j)}$ and $\vec{A}^{(j)}$ are the eigenvalues and the eigenvectors of the related spectral problem, depending on the wavevector $k_x$ (or angle $\theta_o$). The normalization of $\vec{A}^{(j)}$ is such that $\sum_{j=1}^{3} \vec{A}^{(j)} = (1,0,0)^T$ for all wavevectors $k_x$ (angles $\theta_o$). The complex eigenvalues are defined by $k_z^{(j)} = \frac{(u_j - s^2)q_x^2}{2k_0\overline{n}}$, where $u_j(s,v)$ are roots of the cubic polynomial equation:

$$\mathcal{H}(u,s,v) \stackrel{def}{=} u\left[(u-v)^2 - 4s^2\right] - 2c^2(u-v) - 4c^2 b(c+bu) = 0. \tag{11}$$

In the following, we are mainly interested in the shape and evolution of $a_0(z,k_x)$, which is the first component of the vector $\vec{a}$ and represents the central part of the far field around the angle $\theta_o = 0$. The far field around the angles $\theta_o = \frac{q_x}{k_0}$ and $\theta_o = -\frac{q_x}{k_0}$ is represented by the functions $a_{+1}(z,k_x)$ and $a_{-1}(z,k_x)$, respectively.

## 4.1 Modal gain functions

All three roots $u_j(s,v)$ of Eq. (11) can be found by Cardano's formula. We order the roots according to their imaginary parts (modal gain) at $s = 0$, so that $\mathrm{Im}\, u_1(0,v) \geq \mathrm{Im}\, u_2(0,v) \geq \mathrm{Im}\, u_3(0,v)$.

The form of the solution, Eq. (10), suggests that the shape of the beam in wavevector space (far field) is predominantly determined by the modal gain functions $\mathrm{Im}\, k_z^{(j)}$, $j = 1,2,3$. The

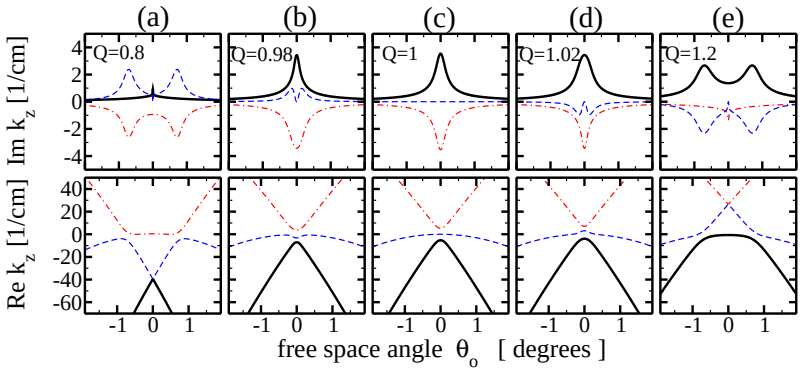


Figure 4: Mode wavevectors $k_z$ of CM equations (9) depending on the angle $\theta_o$, for different values of $\mathcal{Q}$. First row: mode gain/absorption profiles. Second row: the real part of the wavevectors. Columns (a), (b), (c), (d), and (e) represent the cases of $\mathcal{Q} = 0.8, 0.98, 1, 1.02$, and $1.2$, respectively. $b = 0$, $a_m = 10\,\mathrm{cm}^{-1}$, $\alpha_H = 1.5$, whereas $\lambda_0$, $d_x$, and $d_z$ are as given in Table 1.

dependence of the normalized wavevectors $k_z$ on the vector $k_x$ (angle $\theta_o$) in the chessboard-type contact case is depicted in Fig. 4, for five different values of $\mathcal{Q}$. The upper row of this figure predicts that the sharpest far field profiles occur for the geometry factor $\mathcal{Q} \approx 1$: in this case, the main modal gain function (solid curve) has a well pronounced narrow single-headed peak centered at $\theta_o = 0$, whereas the remaining (off-axis) modes are damped [columns (c) and (d)] or only weakly amplified [column (b)].

It is obvious that the desirable effects, far field amplification and the narrowing of its distribution, are more pronounced for a large main modal gain with a sharp peak. At $\theta_o = 0$ (or $s = 0$), the

solutions $u_j$ of the characteristic Eq. (11) for the chessboard-type modulation case ($b = 0$) are given by:

$$u_1(0,v) = \tfrac{v+\mathcal{S}(v)}{2},\ u_2(0,v) = v,\ u_3(0,v) = \tfrac{v-\mathcal{S}(v)}{2},$$
$$\text{where } \mathcal{S}(v) = \sqrt[+]{v^2+8c^2},\ \ \mathrm{Im}\,\sqrt[+]{\xi} \geq 0.$$

Thus, in order to increase the value of the dominant gain function at $\theta_o = 0$, $\mathrm{Im}\, u_1(0,v)$ has to be maximum.

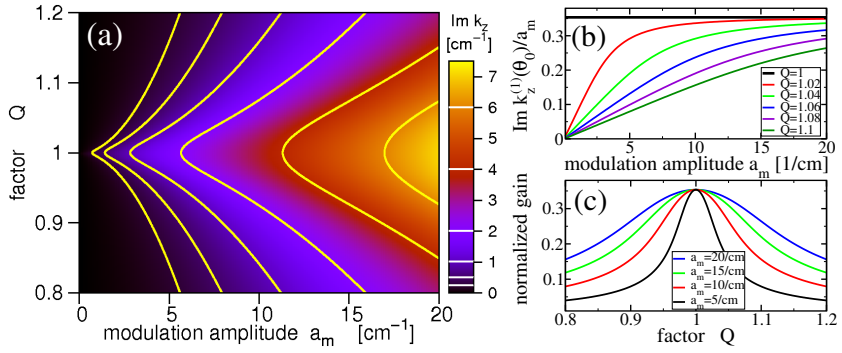


Figure 5: Main mode gain function at $\theta_o = 0$ depending on $a_m$ and $\mathcal{Q}$. $b = 0$, $\alpha_H = 1$, $d_x = 8\,\mu$m.

A standard analysis and Fig. 5 shows how for fixed values of $\alpha_H \neq 0$, $d_x$ and $\mathcal{Q}$ the main mode gain function at $\theta_o = 0$ monotonously grows with the modulation amplitude $a_m$ [see panel (a)]. Panels (b) and (c) of this figure also show that for large values of $a_m$, a modal gain at $\theta_o = 0$ display similar values around $\mathcal{Q} \approx 1$. For $\mathcal{Q} \to 1$, the modal gain value approaches the unique maximum $\frac{|a_m|\sqrt{2}}{4}$.

## 4.2 Contribution of different modes

Note that the peak value of the main gain function for $\mathcal{Q} \approx 1$ and the realistic modulation amplitude $a_m = 10\,\mathrm{cm}^{-1}$ (black solid curves in the upper row of Fig. 4) is moderate: it does not exceed $3.5\,\mathrm{cm}^{-1}$. Hence, in order to double the power of this mode at $\theta_o = 0$, at least a $1$ mm long amplifier is needed. As a typical length of BA amplifiers does not exceed several millimeters, we should be sure that not only the gain but also the initial contribution of the main mode, $A_0^{(1)}$, is sufficiently large comparing it to the contributions $A_0^{(2)}$ and $A_0^{(3)}$ of the other modes.

Figure 6 illustrates the growth and decay of the three low order mode contributions in BA amplifiers, for the different cases considered in Fig. 4. The top row in Fig. 6 shows that the initial contribution of the main mode is more pronounced for $\mathcal{Q} \geq 1$, what results in a clear dominance of this mode after a moderate propagation distance [second row panels of columns (c-e)]. The resulting far field profile (the bottom row panels) in these cases is determined by the main mode and its modal gain width (see solid curves on the top row). As a consequence, the best combined result (sharpest far field) can be expected for $\mathcal{Q}$ factors slightly larger than 1.

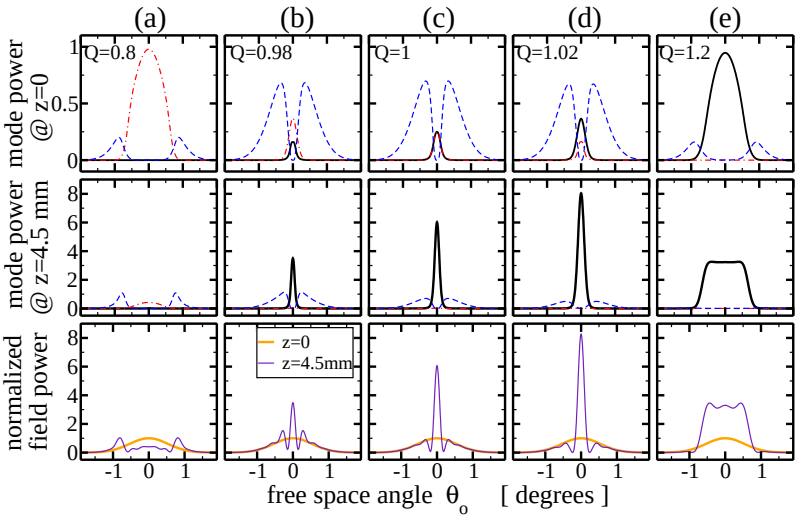


Figure 6: Bloch mode coefficient intensities at $z = 0$ [first row] and $z = 4.5$ mm [second row], and normalized field intensity at $z = 0$ (grey) and $z = 4.5$ mm (black dashed) [third row]. Columns, parameters and line styles as in Fig. 4.

### 4.3 Impact of the linewidth enhancement factor.

Next, we study the role of the modulation of the refractive index (imaginary part of $\beta$). In general, such modulation directly occurs due to the non-vanishing linewidth enhancement factor, $\alpha_H$, see Eq. (8). The index modulation can be additionally introduced through a manipulation of the semiconductor material (e.g., creating regions with different refractive index), represented by the spatial dependence of $\delta_0$ in Eq. (2).

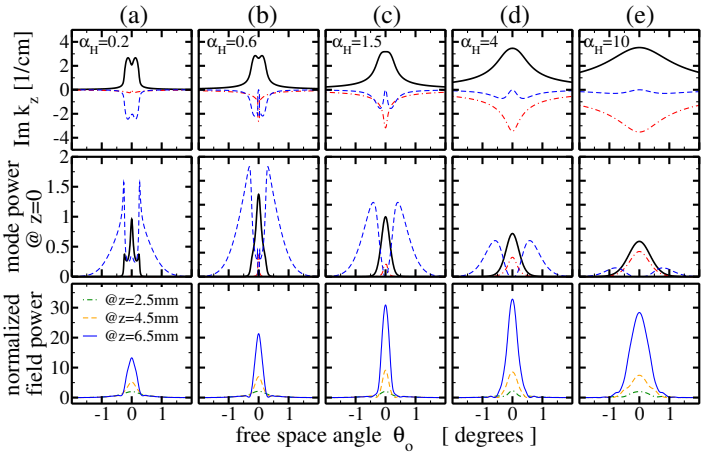


Figure 7: Modal gain functions [first row], initial mode intensities at $z = 0$ [second row], and normalized field intensity at different distances $z$ [third row], for $\alpha_H = 0.2$, $0.6$, $1.5$, $4$, and $10$ [columns (a) to (e)] and $\mathcal{Q} = 1.04$. All other parameters as in Fig. 4.

Figure 7 shows how an increase of the index modulation (increase of linewidth enhancement factor) entails the broadening of the main mode gain profile (solid curves on the top row). Another effect is the broadening of the main mode intensity profile in the mode decomposition of the initial beam (solid curves on the middle row), and decrease of the relative part of the second mode in the same decomposition (dashed curves on the same row). As a consequence, for a large $\alpha_H$ the far field [bottom row panels on columns (c-e)] of the amplifiers with moder-

ate length is predominantly determined by the main mode and its gain. We note, however, that due to the broadening of the gain profile at very large $\alpha_H$ the narrowing of the far field is less effective: see column (e) of the same figure.

For larger $\mathcal{Q}$ the main mode gain has a double-peak structure, what can damage the far field profile: see, e.g., columns (e) of Figs. 4 and 6. The top row of Fig. 7 also evidences that the double-peak gain strongly depends on the alpha-factor.

## 4.4 Topology of the gain functions

A summary of these observations is given in Fig. 8, where we characterize the topology of the main mode gain function and its relation to the gain functions of the other modes. The narrow concave gain function of the main mode which is dominating for all $\theta_o$ can be found within the domain I, which is the region of our interest. When $\mathcal{Q}$ is larger, the peak of the main mode gain splits, for each such $\mathcal{Q}$ forming the monotonous increase or decay regions II and a convex central region III. For smaller $\mathcal{Q}$, the gain of the main mode decays, whereas the gain of the next mode characterized by two sideband peaks takes over (region IV). In both last cases a relatively wide double-peaked far field of the beam emitted by the long amplifier can be expected.

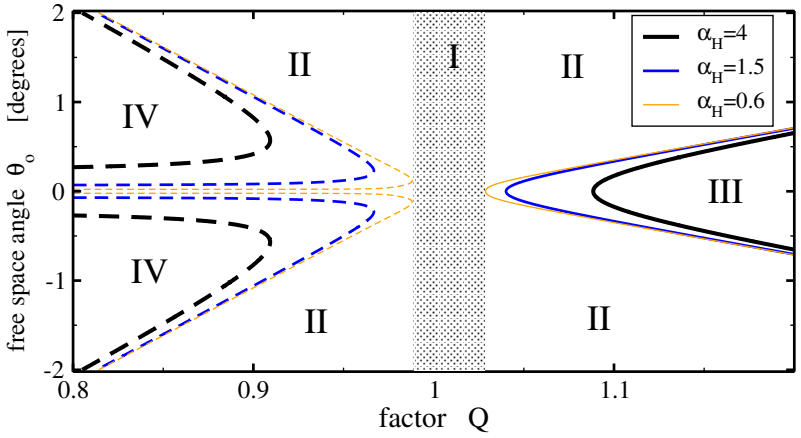


Figure 8: Characterization of the gain profile of the main mode in $\mathcal{Q}$-$\theta_o$ space, for different values of $\alpha_H$. Dashed: gain of the main and the second mode are equal. Solid: peak positions of the double-headed dominant main mode. I, II, and III: parameter regions where dominating main mode is concave, monotonous, and convex, respectively. IV: dominance of other mode. All other parameters as in Fig. 4.

It is noteworthy, that the width of the region I clearly depends on the alpha-factor: see different bands in factor $\mathcal{Q}$ formed by the curves of different thickness in Fig. 8. Therefore, to select an appropriate modal gain profile it would be preferable to design a moderate-to-large $\alpha_H$.

The analysis in this section was performed for the BA amplifiers with the chessboard-type electrodes, separately considering the impact of factors $\mathcal{Q}$, $a_m$, and $\alpha_H$. In the case of the fishnet-type contacts, one should also take into account the impact of the non-vanishing factor $b$ in Eq. (9). This factor, however, should not be treated separately from $a_m$ and $\alpha_H$, but rather

be related to them through the conditions given in Eq. (7) (i.e., all these three parameters are functions of $\bar{J}$, $N_0$ and $d_x$). In this case, the factor $b$ causes only small perturbations of the above discussed mode gain functions $\mathrm{Im}\, k_z^{(j)}(\theta_o)$ as well as initial and final contributions of the modes in the full far field profile. For the comparison of the far field shaping in BA amplifiers with different contacts see also discussion in the following section.

# 5 Simulations

To relate the results of our analysis of the CM approach, Eq. (9), with the beam propagation according to the full and linearized TW model, Eqs. (1)-(5) and Eq. (9), respectively, we have simulated the propagation of a weak Gaussian beam with an initial $20\,\mu$m spatial and $1.264^\circ$ spectral width at half maximum in the BA amplifier using all three approaches considered above.

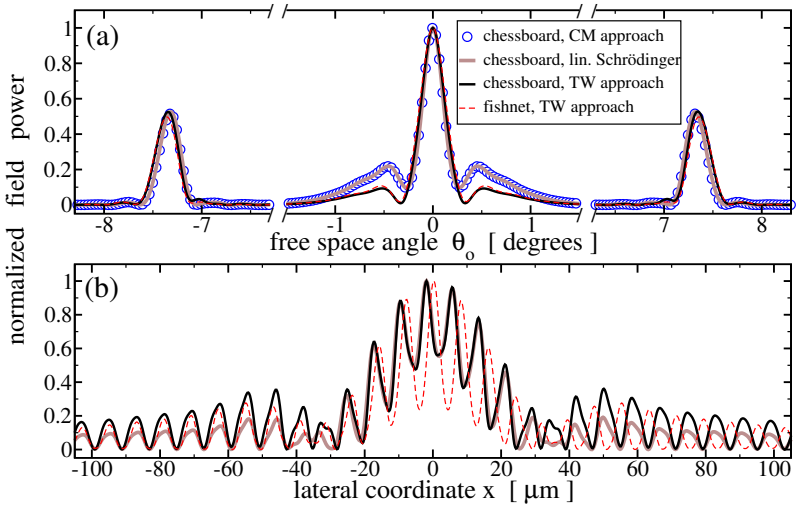


Figure 9: Simulation of a small beam propagation in BA amplifier for chessboard- and fishnet-type contacts. (a): far fields. (b): near fields. The optical fields for chessboard-type contacts are represented by empty bullets [CM approximation (9)], a thick solid gray curve [linear approximation (8)], and a solid thin black curve [TW model (1)-(5)]. A thin dashed curve provides a comparison for the fishnet-type electrodes [TW model (1)-(5)]. In all cases: $\mathcal{Q} = 1.04$, $L = 4.8\,\mu$m, while other parameters are as in Table 1 or derived by means of (7).

First of all, we consider chessboard-type contacts. We note a perfect agreement between the linear approximation and CM approaches. In this case, the function $\hat{E}(L, \theta_o)$ obtained by the numerical integration of Eq. (8) for $z \leq L$ and a consequent far-field transformation of the optical field almost coincides with the analytic solution, Eq. (10), [compare the thick solid gray curve in Fig. 9(a) and the bullets in the same figure]. Namely,

$$\hat{E}(L,\theta_0) \approx \begin{cases} a_{-1}\left(L, \theta_o k_0 + q_x\right) & \text{for } -\frac{3q_x}{2k_0} < \theta_o < -\frac{q_x}{2k_0} \\ a_0\left(L, \theta_o k_0\right) & \text{for } -\frac{q_x}{2k_0} < \theta_o < \frac{q_x}{2k_0} \\ a_{+1}\left(L, \theta_o k_0 - q_x\right) & \text{for } \frac{q_x}{2k_0} < \theta_o < \frac{3q_x}{2k_0} \end{cases} .$$

The near field distributions are shown in Fig. 9(b). In this case, the solution $E(z,x)$ of the linear model (8), and the appropriately scaled stationary solution $E^{+}(z,x,t)$ of the full TW model (1)-(5), exhibit just small differences (compare the solid thick gray and thin black curves). Such discrepancies may be attributed to the limited device width in the TW model, and to the approximation of the step-wise modulated injected current in the longitudinal direction by a harmonic function. However, the basic effect of the narrowing of the central lobe of the far field, remains very similar in both of these simulations, see Fig. 9(a).

Moreover, we note that the far field narrowing effect clearly persists in an analogous BA amplifier electrically pumped through fishnet-type electrodes. While in this later case differences can be also observed in the near field, the far field distributions using TW model approach (1)-(5) almost coincide with those in the chessboard-type case, see the thin dashed curves in Figs. 9(a),(b).

# 6 Conclusions

To conclude, we perform a detailed analysis of the propagation of the field in 2D periodically modulated semiconductor amplifiers of moderate length, and found a significant reduction of the radiation angle and improvement of the beam spatial quality. The system is described by a 2+1 dimensional TW model which is studied within linear and a CM approximations. In the CM approximation, the far field shape is determined by the angular profile of the imaginary parts of the mode wavevectors. We show the existence of amplified modes, which profile depends on the geometry factor $\mathcal{Q}$. For $\mathcal{Q} \approx 1$, the main modal gain function approaches a maximum, has a well pronounced narrow single-headed peak, and monotonously grows with the modulation amplitude. The desirable effects of far field amplification and narrowing are more pronounced for a large main modal gain with a sharp peak. Moreover, the amplitude of the index modulation, governed by the value of the linewidth enhancement factor, $\alpha_H$, also plays an important role. An increase of the index modulation leads to a broadening of the main mode gain profile. As a consequence, for sufficiently large $\alpha_H$, the far field of amplifiers of moderate length is almost fully determined by the main mode and its gain. However, for large $\alpha_H$ the narrowing of the far field is less efficient due to the broadening of the gain profile. Therefore, selecting an appropriate modal gain profile is preferable to have moderate-to-large linewidth enhancement factor. For higher values of $\mathcal{Q}$ the main mode develops a double-peak structure.

To summarize all the observations, we completely characterize the topology of the main mode gain function and its relation with the gain functions of the other modes, determining a region of single-peak mode amplification around $\mathcal{Q} \approx 1$, which broadens with increasing $\alpha_H$. Finally, we perform simulations of weak Gaussian beam propagation within the BA amplifier, either considering the full TW model, its linearized approximation, and the CM approach. In all cases, the same effect of the narrowing of the central lobe of the optical far field is observed. We also show that the effect persists for different configurations of modulated BA amplifiers with analogous geometry, we prove that the more realistic fishnet-type contacts provide similar results as the idealized chessboard-type electrodes.

## Acknowledgement

M. R. would like to acknowledge the support of EU FP7 ITN PROPHET, Grant No. 264687 and SFB 787 of the DFG. The other authors acknowledge the financial support of Spanish Ministerio de Educación y Ciencia and European FEDER through project FIS2011-29734-C02-01, as well as European Union Structural Funds project.

## Appendix

The stationary carrier density $N_{st}(z,x)$ can be written as a sum of harmonic components,

$$N_{st}(z,x) = N_0 + \sum_{(k,l)\in\mathbf{Z}\times\mathbf{Z}\setminus(0,0)} N_{k,l}\, e^{ikq_z z} e^{ilq_x x},$$

where $N_0$ is the mean value of $N_{st}(z,x)$, and $N_{k,l}$ are complex constants satisfying the complex-conjugation condition, $N_{-k,-l} = N^*_{k,l}$. The linearization of the stationary carrier rate equation around spatially averaged density $N_0$,

$$\tfrac{\bar{J}(1+\zeta(z,x))}{qd} \approx R(N_0) + \left[\tfrac{\partial R}{\partial N}(N_0) - D_N \tfrac{\partial^2}{\partial x^2}\right](N_{st} - N_0),$$

allows to identify all the coefficients $N_{k,l}$:

$$N_{k,l} = \tfrac{\bar{J}\zeta_{k,l}}{qd}\left[D_N l^2 q_x^2 + \tfrac{\partial R}{\partial N}(N_0)\right]^{-1}, \quad k,l \in \mathbf{Z},$$
$$\zeta_{k,l} = \tfrac{1}{d_z d_x}\int_0^{d_x}\int_0^{d_z} \zeta(z,x) e^{-ikq_z z} e^{-ilq_x x} dz dx.$$

For the chessboard- and the fishnet-type functions, $\zeta = \zeta^{(ch)}$ and $\zeta = \zeta^{(fn)}$, all non-vanishing coefficients $\zeta_{k,l}$ are real-valued and are given by

$$\zeta^{(ch)}_{k,l} = -\tfrac{4}{kl\pi^2}, \qquad k,l \text{ are odd};$$
$$\zeta^{(fn)}_{k,l} = -\tfrac{8\, i^{k-l}}{\pi^2}\, \tfrac{\sin(\frac{\pi(k+l)\sqrt{2}}{4})}{k+l}\, \tfrac{\sin(\frac{\pi(k-l)\sqrt{2}}{4})}{k-l}, \quad k-l \text{ is even}.$$

It is noteworthy, that in both cases the conditions $\zeta_{k,l} = \zeta_{l,k}$ and $\zeta_{k,l} = (-1)^k \zeta_{-k,l}$ hold for all $k,l \in \mathbf{Z}$.

The linearization of the stationary propagation factor $\beta(N_{st}(z,x),0)$ around $N_0$ yields

$$\beta(N_{st},0) \approx \beta(N_0,0) + \tfrac{g' N_{\mathrm{tr}}}{2N_0}\left(1 + i\tfrac{k_0\sqrt{\mu N_0}}{g' N_{\mathrm{tr}}}\right)(N_{st} - N_0).$$

The restriction of the harmonic expansion of $N_{st} - N_0$ to the components with $|k| + |l| \leq 2$ in both considered cases of function $\zeta$ implies the expressions of $a_m$, $\alpha_H$, potential $V(z,x)$ and factors $b$, $b_z$ in Eq. (7).

# References


[1] P. Chazan, J.M. Mayor, S. Morgott, M. Mikulla, R. Kiefer, S. Müller, M. Walther, J. Braunstein and G. Weimann. High-power near difraction-limited tapered amplifiers at 1064 nm for optical intersatelite communications. *IEEE Phot. Techn. Lett.*, **10**(11):1542–1544, 1998.

[2] M. Maiwald, S. Schwertfeger, R. Güther, B. Sumpf, K.Paschke, C. Dzionk, G. Erbert and G. Tränkle. 600 mW optical output power at 488 nm by use of a high-power hybrid laser diode system and a periodically poled MgO:$LiNbO_3$. *Optics Letters*, **31**(6):802–804, 2006.

[3] W. Schultz and R. Poprawe. Manufacturing with nover high-power diode lasers. *IEEE J. Select. Topics Quantum Electron.*, **6**(4):696–705, 2000.

[4] M. Pessa, J. Näppi, P. Savolainen, M. Toivonen, R. Murison, A. Ovchinnikov and H. Asonen. State-of-the-art aluminum-free 980-nm laser diodes. *J. Ligthw. Technol.*, **14**(10):2356–2361, 1996.

[5] T. Burkhard, M.O. Ziegler, I. Fischer, and W. Elsäßer. Spatio-temporal dynamics of broad area semiconductor lasers and its characterization. *Chaos Solitons Fractals*, **10**:845–850, 1999.

[6] G. R. Hadley, A. Owyoung, and J. P. Hohimer. Modeling of injection-locking phenomena in diode-laser arrays. *Optics Letters*, **11**(3):144–146, 1986.

[7] M. Radziunas and K. Staliunas. Spatial rocking in broad area semiconductor lasers. *Europhysics Letters*, **95**:14002, 2011.

[8] A. Jechow, M. Lichtner, R. Menzel, M. Radziunas, D. Skoczowsky, and A. Vladimirov. Stripe-array diode-laser in an off-axis external cavity: Theory and experiment. *Europhysics Letters*, **95**:14002, 2011.

[9] M. Lichtner, V.Z. Tronciu, A.G. Vladimirov. Theoretical investigation of striped and non-striped broad area lasers with off-axis feedback. *IEEE J. of Quantum Electron.*, **48**(3):353–360, 2012.

[10] R. Herrero, M. Botey, M. Radziunas, and K. Staliunas. Beam shaping in spatially modulated broad area semiconductor amplifiers. *Optics Letters*, **37**(24):5253–5255, 2012.

[11] M. Radziunas, M. Botey, R. Herrero, and K. Staliunas. Intrinsic beam shaping mechanism in spatially modulated broad area semiconductor amplifiers. *Appl. Phys. Letters*, **103**(13):132101, 2013.

[12] S. Balsamo, F. Sartori and I. Montrosset. Dynamic beam propagation method for flared semiconductor power amplifiers. *IEEE Journal of Selected Topics in Quantum Electronics*, **2**:378–384, 1996.

[13] M. Spreemann, M. Lichtner, M. Radziunas, U. Bandelow and H. Wenzel. Measurement and simulation of distributed-feedback tapered master-oscillators power-amplifiers. *IEEE J. of Quantum Electron.*, **45**(6):609–616, 2009.

[14] U. Bandelow, M. Radziunas, J. Sieber and M. Wolfrum. Impact of gain dispersion on the spatio-temporal dynamics of multisection lasers. *IEEE J. of Quantum Electron.*, **37**:183–188, 2001.